Phononic entanglement concentration via optomechanical interactions

Shan-Shan Chen,[1] Hao Zhang,[1,2,*] Qing Ai,[1] and Guo-Jian Yang[1,†]

[1]*Department of Physics, Applied Optics Beijing Area Major Laboratory, Beijing Normal University, Beijing 100875, China*

[2]*State Key Laboratory of Low-Dimensional Quantum Physics, Department of Physics, Tsinghua University, Beijing 100084, China*

(Received 24 August 2019; published 5 November 2019)

Low-dissipation, tunable coupling to other quantum systems and unique features of phonons in the aspects of propagation, detection, and other areas suggest the applications of quantized mechanical oscillators in phonon-based quantum information processing (QIP) in a way different from their photonic counterpart. In this paper, we propose a protocol of entanglement concentration for nonlocal phonons from quantized mechanical vibration. We combine the optomechanical cross-Kerr interaction with the Mach-Zehnder interferometer and, by means of twice optomechanical interactions and the photon analysis with respect to the output of the interferometer, achieve ideal entanglement concentration about less-entangled nonlocal phonon Bell and Greenberger-Horne-Zeilinger states. Our protocol is useful for preserving the entangled phonons for the use of high-quality phonon-based QIP in the future.

DOI: 10.1103/PhysRevA.100.052306

I. INTRODUCTION

Quantum entanglement is a quantum resource indispensable in some areas, such as quantum key distribution [1–3], quantum teleportation [4], quantum secure direct communication [5–8], and quantum dense coding [9,10]. In quantum communications, an entangled state is usually used for building a quantum channel between remote parties. However, the channel noise will induce decoherence and degrade the entanglement between the quantum systems. Entanglement concentration [11–25] is an operation which converts a partially entangled state to a more or a maximally entangled state. Since the first entanglement concentration protocol (ECP), the well-known Schmidt projection, was proposed by Bennett *et al.* [11], its realization on various physical systems has been reported. Examples include ECPs with linear optical elements in the principle of Schmidt projection [12,13], nonlocal-photon ECP with linear [17] or nonlinear optical elements [19,20], and ECP based on electron-spin systems [21] or on circuit quantum electrodynamics [22,23], etc.

Mechanical resonators are known as important platforms on which one can generate different quantum effects [26–32] and realize quantum information processing (QIP) [33,34]. As the information carriers of quantized mechanical vibration modes, phonons can be confined in mechanical resonators and propagate in phononic waveguides [35–38]. Compared to photons, the phonons' speed is much slow, thus they are more suitable for storing and transferring quantum information between quantum nodes over a short distance. With the development of the technique of phononic crystals, which can effectively enhance the mechanical Q-factor [35,36], and due to the distinct advantages with low dissipation and tunable coupling to other systems, mechanical resonators and their complex, such as optomechanical systems [33,34,39–45] and hybrid solid phonon-spin systems [46–50], have been applied to storage, transducers, and sensors in QIP [51–54] and to the building of scaling-on-chip phononic quantum networks [55,56].

Phonon entanglement is generated with quantized mechanical vibration modes, and, on this subject, there are already some important works [28,30–32]. In this paper we focus on how to preserve the phonon entanglement based on the concept of entanglement concentration. Most existing ECPs were designed for photons, which work with linear or nonlinear optical elements and photon-detectable instruments. Because there are not phononic linear elements, phonons cannot be operated as photons can, and the photonic ECPs do not apply to the phonons. In the present investigation, we propose the first ECP for entangled nonlocal phonons. In this protocol, phonons are operated indirectly by controlling photons via optomechanical interaction, so that the original partially entangled two-phonon state is converted to the Bell state or, similarly, a partially entangled three-phonon state to the Greenberger-Horne-Zeilinger (GHZ) state. In detail, three steps need to take place in our ECP. In step 1, using the combination of a cross-Kerr optomechanical system with a Mach-Zehnder interferometer, we obtain the maximally entangled phonon state with a certain successful probability, where the dimension of this phonon state is two times as large as that of the original state to be concentrated for entanglement. In step 2, using the second optomechanical interaction to drive the anti-Stokes transition, we map the state of the whole system onto a phonon-photon state. After all the users make the X-basis measurement on their own photons in step 3 as well as share the measurement results, we complete the entanglement concentration about that less-entangled multiphonon state.

This article is organized as follows: In Sec. II we give a description of the protocol and show how a partially entangled nonlocal two-phonon state becomes a Bell state by applying our ECP. In Sec. III we extend our ECP to the multiuser GHZ

*zhanghaoguoqing@163.com
†yanggj@bnu.edu.cn

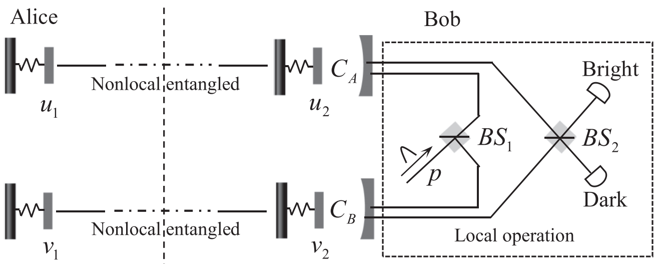

FIG. 1. Schematic diagram of step 1 used in the ECP. u_j (v_j) ($j = 1, 2$) are four mechanical oscillators, among which u_2 (v_2) acts as the end mirror of the Fabry-Pérot cavity C_A (C_B). BS_1 is a beam splitter through which a photon p is sent into C_A and C_B at equal probability. Beam splitter BS_2 together with BS_1 and two cavities constitute a Mach-Zehnder interferometer used for orthogonal postselection. The dotted box represents a local operation on phonons u_2 and v_2 to postselect the maximally entangled four-phonon state, realized by Bob through directly controlling the photons via the optomechanical interaction. All elements on the left of the vertical dashed line are used by Alice, and those on the right by Bob.

state and give two simple remarks about the feasibility of our protocol. A summary is given in Sec. IV.

II. ENTANGLEMENT CONCENTRATION FOR PARTIALLY ENTANGLED NONLOCAL PHONONS

We assume that the partially entangled nonlocal phonons under the consideration of entanglement concentration are in a state shared by two remote mechanical oscillators b_1 and b_2, and fulfils

$$|\psi\rangle_{b_1b_2} = \alpha|10\rangle_{b_1b_2} + \beta|01\rangle_{b_1b_2}, \tag{1}$$

with $|\alpha|^2 + |\beta|^2 = 1$, where $|i_1i_2\rangle_{b_{j_1}b_{j_2}}$ ($i_1, i_2 = 0, 1$ and $j_1, j_2 = 1, 2$) is the phonon number state with i_1 phonons in the oscillator mode b_{j_1} and i_2 phonons in the oscillator mode b_{j_2}. For simplicity, we have used the abbreviation $|i_1\rangle_{b_{j_1}}|i_2\rangle_{b_{j_2}}\cdots|i_k\rangle_{b_{j_k}} = |i_1i_2\cdots i_k\rangle_{b_{j_1}b_{j_2}\cdots b_{j_k}}$ to compact the expression of a multimode state of oscillators. This is also applied to the expression of a multimode state of optical cavities, but we always write a phonon state separately with a photon state. State (1) results from the decoherence of the ideal Bell state $|\psi\rangle_{b_1b_2} = \frac{1}{\sqrt{2}}(|10\rangle_{b_1b_2} + |01\rangle_{b_1b_2})$ (see the Appendix for the generation of this state) due to the mechanical oscillators b_1 and b_2 operating in dissipative environments or interacting with other quantum systems. The target state after concentration is that with $\alpha = \beta = \frac{1}{\sqrt{2}}$. Three steps are designed in our phononic ECP. In step 1 as shown by Fig. 1, at the beginning, Alice and Bob share two pairs of partially entangled nonlocal oscillator modes u_1v_1 and u_2v_2 described by the states

$$\begin{aligned}|\psi\rangle_{u_1u_2} &= \alpha|10\rangle_{u_1u_2} + \beta|01\rangle_{u_1u_2},\\ |\psi\rangle_{v_1v_2} &= \alpha|10\rangle_{v_1v_2} + \beta|01\rangle_{v_1v_2}.\end{aligned} \tag{2}$$

These two states have forms which are the same as that of state $|\psi\rangle_{b_1b_2}$, Eq. (1), among which, for description convenience, $|\psi\rangle_{u_1u_2}$ is now the state to be concentrated, and $|\psi\rangle_{v_1v_2}$ is the auxiliary phonon state for the use of assisting concentration. Then Bob makes a local operation with respect to his two phonons u_2, v_2 and, finally, the postselection of the maximally entangled four-phonon state, by performing single-photon postselection through the optomechanical interaction. Here the cross-Kerr optomechanical interaction [57–59] between the cavity and the mechanical oscillator is used to meet the requirement of Bob's operation. This interaction can be obtained through the direct optomechanical quadratic coupling or the enhanced cross-Kerr coupling between photon and phonon by using an auxiliary mechanical oscillator [59]. The Hamiltonian can be written correspondingly as the universal form

$$H = \omega_c c^\dagger c + \omega_m b^\dagger b - g c^\dagger c b^\dagger b, \tag{3}$$

where $c^\dagger(c)$ is the creation (annihilation) operator for the cavity and $b^\dagger(b)$ for the mechanical oscillator, with ω_c and ω_m their effective frequencies, respectively. g denotes the effective coupling between modes c and b. With Hamiltonian (3), the Fock state of a phonon-photon system evolutes with the phase accumulation as follows:

$$\begin{aligned}|0\rangle_c|0\rangle_b &\longrightarrow |0\rangle_c|0\rangle_b,\\ |0\rangle_c|1\rangle_b &\longrightarrow e^{-i\theta_{01}}|0\rangle_c|1\rangle_b,\\ |1\rangle_c|0\rangle_b &\longrightarrow e^{-i\theta_{10}}|1\rangle_c|0\rangle_b,\\ |1\rangle_c|1\rangle_b &\longrightarrow e^{-i\theta_{11}}|1\rangle_c|1\rangle_b,\end{aligned} \tag{4}$$

where $|0\rangle_c$ ($|1\rangle_c$) and $|0\rangle_b$ ($|1\rangle_b$) represent the ground (first excited) state of cavity mode c and mechanical oscillator mode b, respectively. Here we have introduced the phases $\theta_{01} = \omega_m t$, $\theta_{10} = \omega_c t$ and $\theta_{11} = (\omega_m + \omega_c - g)t$.

By applying operation (4) to state (2), that is, as shown in Fig. 1, letting a photon entering the cavity A or B, the state of the whole phonon-photon system will evolve into

$$\begin{aligned}|\psi(t)\rangle = &\frac{1}{\sqrt{2}}(|10\rangle_{AB} + |01\rangle_{AB}) \otimes (\alpha|10\rangle + \beta|01\rangle)_{u_1u_2}\\ &\times \otimes (\alpha|10\rangle + \beta|01\rangle)_{v_1v_2},\\ \longrightarrow\ &\frac{1}{\sqrt{2}}[|10\rangle_{AB} \otimes (\alpha e^{-i\theta_{10}}|10\rangle + \beta e^{-i\theta_{11}}|01\rangle)_{u_1u_2}\\ &\times \otimes (\alpha|10\rangle + \beta e^{-i\theta_{01}}|01\rangle)_{v_1v_2}\\ &+|01\rangle_{AB} \otimes (\alpha|10\rangle + \beta e^{-i\theta_{01}}|01\rangle)_{u_1u_2}\\ &\times \otimes (\alpha e^{-i\theta_{10}}|10\rangle + \beta e^{-i\theta_{11}}|01\rangle)]_{v_1v_2},\end{aligned} \tag{5}$$

where $|i_1i_2\rangle_{AB}$ ($i_1, i_2 = 0, 1$) means the photon state with i_1 (i_2) photons in cavity A (B). If a photon is detected at the dark port after the second beam splitter BS_2, an orthogonal postselection is performed with the single-photon state $|\psi\rangle_f = \frac{1}{\sqrt{2}}(|10\rangle_{AB} - |01\rangle_{AB})$. Then, the final state for the mechanical oscillators becomes

$$\begin{aligned}|\psi\rangle_1 = &\tfrac{1}{2}\big[(\alpha e^{-i\theta_{10}}|10\rangle + \beta e^{-i\theta_{11}}|01\rangle)_{u_1u_2}\\ &\otimes(\alpha|10\rangle + \beta e^{-i\theta_{01}}|01\rangle)_{v_1v_2}\\ &-(\alpha|10\rangle + \beta e^{-i\theta_{01}}|01\rangle)_{u_1u_2}\\ &\otimes(\alpha e^{-i\theta_{10}}|10\rangle + \beta e^{-i\theta_{11}}|01\rangle)\big]_{v_1v_2}\\ = &\tfrac{1}{2}\alpha\beta\xi(t)(|1001\rangle - |0110\rangle)_{u_1u_2v_1v_2},\end{aligned} \tag{6}$$

where $\xi(t)$ is $\xi(t) = e^{-i(\omega_m+\omega_c)t}(1 - e^{igt})$. Therefore, the maximally entangled state between four mechanical oscillators u_1,

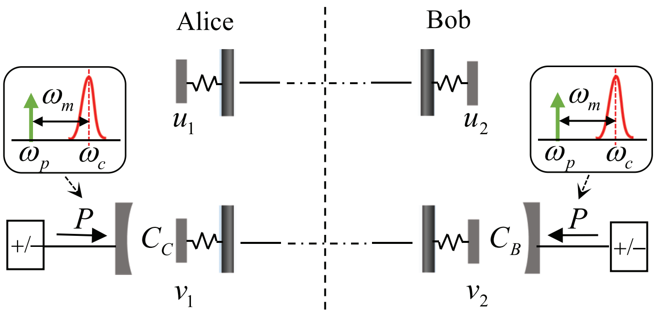

FIG. 2. Schematic diagram of steps 2 and 3 in the ECP. u_j (v_j) ($j = 1, 2$) are four mechanical oscillators, among which v_1 (v_2) acts as the end mirror of the Fabry-Perot cavity C_C (C_B). Letter P means the input pump laser used for driving the anti-Stokes sideband interaction in the photon-phonon systems. The inset shows the frequency relationship between the pump field (green arrow) and the cavity mode (dash red line). The sign $+/-$ represents the X-basis measurement of a photon in step 3. All elements on the left of vertical dashed line are used by Alice, and those on the right by Bob.

u_2, v_1, and v_2,

$$|\psi\rangle_2 = \frac{1}{\sqrt{2}}(|1001\rangle - |0110\rangle)_{u_1u_2v_1v_2}, \tag{7}$$

can be obtained with successful probability

$$P = 2|\alpha\beta|^2 \sin^2\left(\frac{gt}{2}\right). \tag{8}$$

At time $t = \frac{(2n_1+1)\pi}{g}$ [59], we can get the maximal probability

$$P_{\max} = 2|\alpha\beta|^2. \tag{9}$$

In step 2, as shown in Fig. 2, two red-detuned pump pulses are input to cavities B and C to drive the anti-Stokes transition, respectively. In this process, an anti-Stokes photon is emitted with annihilating a phonon. In fact, it has been well realized experimentally to transform a phonon into a photon via an anti-Stokes process [32]. The corresponding interaction Hamiltonian is

$$H_{as} = Gc_jv_j^\dagger + \text{H.c.}, \tag{10}$$

where c_j ($j = 1, 2$) is the photon annihilation operator of the cavity mode C if $j = 1$ or B if $j = 2$, and v_j ($j = 1, 2$) is the phonon annihilation operator of the oscillator mode v_j. G is the coupling strength between the jth mechanical oscillator and the driven cavity after linearizing treatment. With this Hamiltonian, the mechanical oscillator state, Eq. (7), can then be mapped onto a phonon-photon state

$$|\psi\rangle_3 = \frac{1}{\sqrt{2}}(|10\rangle_{u_1u_2}|01\rangle_{CB} - |01\rangle_{u_1u_2}|10\rangle_{CB}). \tag{11}$$

In step 3, as shown in Fig. 2, Alice and Bob make the X-basis measurement with the diagonal basis $\{|\pm\rangle = \frac{1}{\sqrt{2}}(|0\rangle \pm |1\rangle)\}$ on photons C and B, respectively. After this, the ECP is accomplished. What they obtain is the maximally entangled phonon state

$$|\psi\rangle_4 = \frac{1}{\sqrt{2}}(|10\rangle_{u_1u_2} + |01\rangle_{u_1u_2}), \tag{12}$$

TABLE I. The core steps of the ECP.

Step	Process
1	Postselect maximally entangled four-phonon state
2	Transfer phonons to photons via anti-Stokes process
3	Make X-basis measurement on photons

if their measurement results are different, or

$$|\psi\rangle_5 = \frac{1}{\sqrt{2}}(|10\rangle_{u_1u_2} - |01\rangle_{u_1u_2}), \tag{13}$$

if their measurement results are the same. The phonon state $|\psi\rangle_5$ can be transferred to $|\psi\rangle_4$ via a π-phase operation about any one of the phonons. All the steps of entanglement concentration shown above are listed in Table I.

III. ENTANGLEMENT CONCENTRATION FOR LESS-ENTANGLED GHZ STATE OF PHONONS

In this section we extend the above investigation of the two-oscillator case over the multiresonator one and consider how a less-entangled GHZ state of phonons is concentrated for entanglement. Figure 3 is the schematic diagram of the scheme, where the mechanical oscillator x_j (y_j) belongs to Alice if $j = 1$, Bob if $j = 2$, and Charlie if $j = 3$. Initially, Alice, Bob, and Charlie share two pairs of less-entangled tripartite GHZ states

$$\begin{aligned} |\varphi\rangle_{x_1x_2x_3} &= \alpha|000\rangle_{x_1x_2x_3} + \beta|111\rangle_{x_1x_2x_3}, \\ |\varphi\rangle_{y_1y_2y_3} &= \alpha|000\rangle_{y_1y_2y_3} + \beta|111\rangle_{y_1y_2y_3}, \end{aligned} \tag{14}$$

with $|\alpha|^2 + |\beta|^2 = 1$. First, Bob combines the optomechanical cross-Kerr interaction with the Mach-Zehnder interferometer

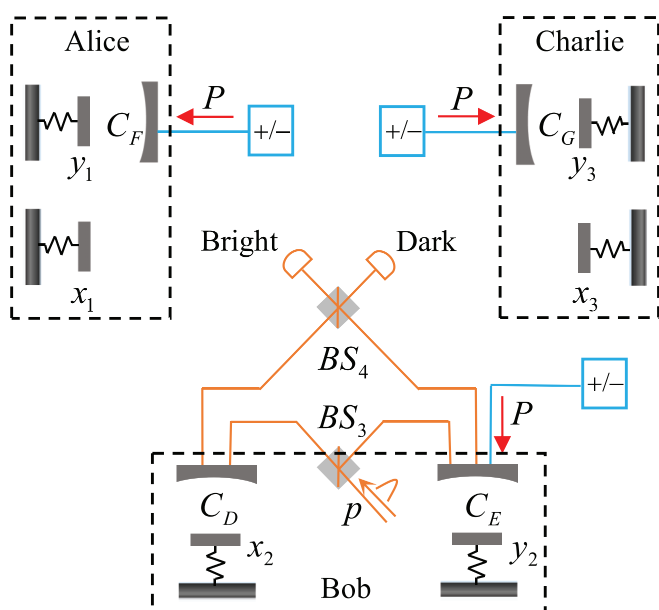

FIG. 3. Schematic diagram of the ECP for phonon GHZ states. The ECP is divided into three parts (see dashed-line long squares) held by Alice, Bob, and Charlie, respectively. The function of Alice's or Charlie's part is the same as that of Alice or Bob in Fig. 2, and the function of Bob's part is the same as that of Bob in Fig. 1.

to realize the maximal entanglement between the six mechanical oscillators by detecting an output photon at the dark port. A photon is then sent to the interferometer of BS_3, and its state after BS_3 becomes $|\varphi\rangle_{\rm in} = \frac{1}{\sqrt{2}}(|10\rangle_{DE} + |01\rangle_{DE})$. When a photon enters cavity D or E, the composite state of the system will evolve to

$$\begin{aligned}|\varphi(t)\rangle &= |\varphi\rangle_{\rm in} \otimes |\varphi\rangle_{x_1x_2x_3} \otimes |\varphi\rangle_{y_1y_2y_3}\\ \longrightarrow\quad & \frac{1}{\sqrt{2}}\big[|10\rangle_{DE} \otimes \big(\alpha e^{-i\theta_{10}}|000\rangle_{x_1x_2x_3} + \beta e^{-i\theta_{11}}|111\rangle_{x_1x_2x_3}\big)\\ & \times \otimes \big(\alpha|000\rangle_{y_1y_2y_3} + \beta e^{-i\theta_{01}}|111\rangle_{y_1y_2y_3}\big)\\ & + |01\rangle_{DE} \otimes \big(\alpha|000\rangle_{x_1x_2x_3} + \beta e^{-i\theta_{01}}|111\rangle_{x_1x_2x_3}\big)\\ & \times \otimes \big(\alpha e^{-i\theta_{10}}|000\rangle_{y_1y_2y_3} + \beta e^{-i\theta_{11}}|111\rangle_{y_1y_2y_3}\big)\big].\end{aligned} \tag{15}$$

If an output photon is detected at the dark port, the single-photon state $|\varphi\rangle_f = \frac{1}{\sqrt{2}}(|10\rangle_{DE} - |01\rangle_{DE})$ is postselected. The final state of the six mechanical oscillators is

$$\begin{aligned}|\varphi\rangle_1 &= \tfrac{1}{2}\alpha\beta e^{-i(\omega_m+\omega_c)t}(1-e^{igt})\\ &\times \big(|000111\rangle_{x_1x_2x_3y_1y_2y_3}\\ &- |111000\rangle_{x_1x_2x_3y_1y_2y_3}\big).\end{aligned} \tag{16}$$

The maximally entangled state can be obtained with a successful probability of postselection, Eq. (8), and reads

$$\begin{aligned}|\varphi\rangle_2 = \frac{1}{\sqrt{2}}\big(&|000111\rangle_{x_1x_2x_3y_1y_2y_3}\\ &-|111000\rangle_{x_1x_2x_3y_1y_2y_3}\big).\end{aligned} \tag{17}$$

At time $t = \frac{2(n_1+1)\pi}{g}$, the successful probability becomes maximal as shown by Eq. (9).

Second, each of these three cavities E, F, and G is pumped with an anti-Stokes light, respectively, to project the mechanical state into the optical cavity state:

$$\begin{aligned}|\varphi\rangle_3 = \frac{1}{\sqrt{2}}\big(&|000\rangle_{x_1x_2x_3}|111\rangle_{EFG}\\ &-|111\rangle_{x_1x_2x_3}|000\rangle_{EFG}\big).\end{aligned} \tag{18}$$

Here $|i\rangle_{c_j}$ ($i = 0, 1$ and $j = 2, 3, 4$ for $c_2 = E$, $c_3 = F$, and $c_4 = G$) is the projected Fock state of i photon in cavity c_j. Then all the users make the X-basis measurement on their photons. If the measurement result is odd number of $|-\rangle$, the state of the mechanical oscillators collapses to

$$|\varphi\rangle_4 = \frac{1}{\sqrt{2}}\big(|000\rangle_{x_1x_2x_3} + |111\rangle_{x_1x_2x_3}\big). \tag{19}$$

On the contrary, if the measurement result is even number of $|-\rangle$, the state becomes

$$|\varphi\rangle_5 = \frac{1}{\sqrt{2}}\big(|000\rangle_{x_1x_2x_3} - |111\rangle_{x_1x_2x_3}\big). \tag{20}$$

The phonon state (20) can be transferred to state (19) and vice versa via a π-phase operation performed by any one of these three users with phonons. By now, we have accomplished the entanglement concentration for the less-entangled GHE state (14).

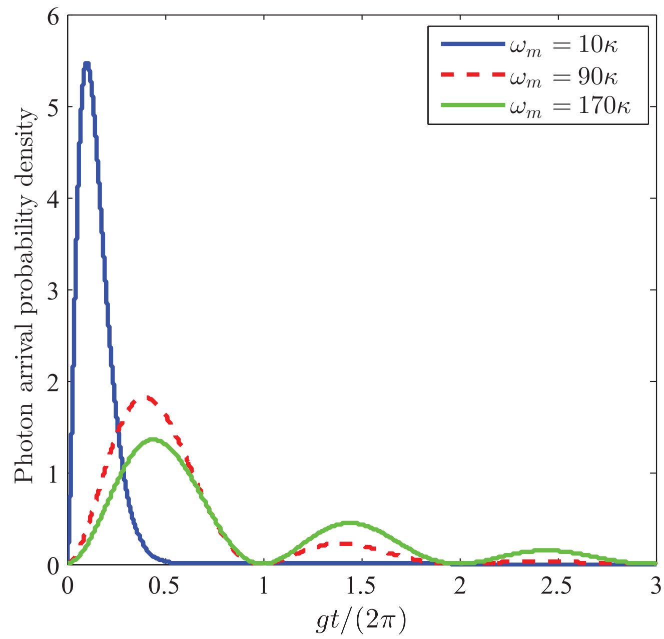

FIG. 4. Photon arrival probability density vs arrival time scaled by $\frac{g}{2\pi}$ for a successful postselection in the sideband-resolved regime $\omega_m = 10\kappa$ (solid green line), $\omega_m = 90\kappa$ (dashed red line), and $\omega_m = 170\kappa$ (solid blue line). Here $\omega_m = 2\pi$ GHz, $g = 3.33 \times 10^{-2}\omega_m$.

Before ending this section, we make two remarks regarding the experimental feasibility about our protocol. The first is that in our protocol, the optomechanical interaction plays an essential role, because the quantum nondemolition measurement and the gate operations of phonons require that the mechanical oscillators must be operated indirectly, while this could easily be achieved via optomechanical interaction. Recent investigations have confirmed the possibility of the above phonon operation by applying the cross-Kerr effect between photons and phonons via optomechanical interaction [57–59]. Second, it is stated that photon-postselection performed at the dark port of a beam splitter in step 1 is an important operation of the ECP for the multiuser GHZ state. We can use the quantity the photon arrival probability density (PAPD) to estimate the probability of a successful postselection. The PAPD can be calculated based on the formula [60]

$$\frac{2|\alpha\beta|^2 \sin^2\left(\frac{gt}{2}\right)\kappa e^{-\kappa t}}{P_{tot}}, \tag{21}$$

where t is the time after the photon releasing from an optical cavity, κ the decay of the cavity, $\kappa exp(-\kappa t)$ the probability density of a photon, and $2|\alpha\beta|^2\sin^2(\frac{gt}{2})$ the probability of a successful postselection at t. P_{tot} is the overall single photon probability for creating the state $|\psi_2\rangle$ shown by Eq. (7) and is described by [60]

$$P_{tot} = 2|\alpha\beta|^2\kappa\int_0^\infty \sin^2\left(\frac{gt}{2}\right)e^{-\kappa t}\,dt = |\alpha\beta|^2\frac{g^2}{g^2+\kappa^2}. \tag{22}$$

We plot the PAPD versus dimensionless arrival time $\frac{gt}{2\pi}$ in Fig. 4. It is shown that $\omega_m \geqslant 90\kappa$ should be satisfied to obtain the observable oscillations of the arrival rate in an optomechanical cavity. The scheme should work in the resolved-sideband regime if the noises from the dark count rate of the detector are taken into consideration. For instance, as we choose $\omega_m = 2\pi$ GHz, which can be realized by a suspended bulk acoustic resonator [32], $g = 3.33 \times 10^{-2}\omega_m$, and $\kappa = 1/90\omega_m$, the probability of the successful postselection, Eq. (22), is approximately $0.8997|\alpha\beta|^2$. The window for detectors receiving photons is approximately $1/\kappa$, and thus the dark count rate should be less than $0.8997|\alpha\beta|^2\kappa$. The current best silicon avalanche photodiodes have a dark count rate of $\sim$2 Hz, which means that $|\alpha\beta|^2 \geqslant 3.184 \times 10^{-8}$ is need to be satisfied for the optomechanical device with $\omega_m = 90\kappa$.

IV. SUMMARY

In summary, we proposed a protocol for nonlocal-phonon entanglement concentration for both the Bell state and the GHZ state. We use the optomechanical cross-Kerr interaction and the Mach-Zehnder interferometer to postselect two phonon pairs with maximally entangled states by detecting the photon output at the dark port of the interferometer. After transforming phonons to photons via another optomichanical interaction and making the Bell-state analysis, we obtain the maximally entangled phonon states shared by nonlocal users, such as the Bell state and the GHZ state, by making the Bell-state analysis. Entanglement is a basic resource for various QIPs, and our work is useful in realizing those phonon-based QIPs.

ACKNOWLEDGMENTS

This work is supported by National Natural Science Foundation of China under Grants No. 11654003 and No. 11174040, the Fundamental Research Funds for the Central Universities (2017TZ01), and the Interdiscipline Research Funds of Beijing Normal University. H.Z. acknowledges the China Postdoctoral Science Foundation under Grant No. 2019M650620.

APPENDIX: ENTANGLEMENT PREPARATION FOR TWO REMOTE MECHANICAL RESONATORS

Reference [32] reported experimental generation of entanglement between nonlocal phonons with two remote optomechanical systems. We present in this Appendix the theoretical model about the Bell-state generation for nonlocal mechanical oscillators. Assume two separate optomechanical systems owned by Alice and Bob are set symmetrically (see Fig. 5). Each of them consists of an optical cavity and a mechanical oscillator and is driven by a pump pulse near the

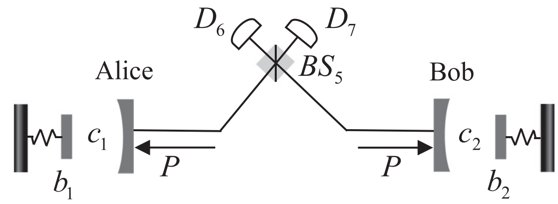

FIG. 5. Schematic diagram of entanglement creation for nonlocal phonons. Two pump pulses described by letter P are input to realize a squeezing interaction between the mechanical mode b_i and the optical mode c_i ($i = 1, 2$) in the optomechanical systems shared by Alice and Bob, respectively.

blue sideband of the cavity to stimulate the Stokes process. After the standard linearization procedure, the corresponding interaction Hamiltonian can be written as

$$H_s = G c_i^\dagger b_i^\dagger + \text{H.c.}, \tag{A1}$$

where $c_i^\dagger$ and $b_i^\dagger$ ($i = 1, 2$) represent, respectively, the creation operators for the ith cavity photon and the ith mechanical oscillator, and $G = g_0\sqrt{n}$ is the effective linear coupling strength which can be varied by changing the intracavity photon number n and the single-photon coupling g_0. With the low-energy pump pulse [32], the composite state of these two optomechanical systems is described by

$$\begin{aligned} |\phi\rangle_1 \otimes |\phi\rangle_2 = &\big(|0\rangle_{c_1}|0\rangle_{b_1} + \sqrt{p_p}c_1^\dagger b_1^\dagger|0\rangle_{c_1}|0\rangle_{b_1}\big) \\ &\otimes\big(|0\rangle_{c_2}|0\rangle_{b_2} + \sqrt{p_p}c_2^\dagger b_2^\dagger|0\rangle_{c_2}|0\rangle_{b_2}\big), \end{aligned} \tag{A2}$$

where $|j\rangle_{c_i}$ ($|j\rangle_{b_i}$) ($i = 1, 2$ or $j = 0, 1$) represent j photons in the cavity mode c_i (j phonons in the oscillator mode b_i). The optomechanical system with subscript i is held by Alice if $i = 1$ or by Bob if $i = 2$. The scattered Stokes photons from two optomechanical systems interfere at beam splitter BS_5 with relation $c_\pm = (c_1 \pm c_2)/\sqrt{2}$. After the BS_5, the composite state will evolve to

$$|\phi\rangle_1 \otimes |\phi\rangle_2 = \sqrt{p_p}\left[\frac{1}{\sqrt{2}}c_+^\dagger(b_1^\dagger + b_2^\dagger) + \frac{1}{\sqrt{2}}c_-^\dagger(b_1^\dagger - b_2^\dagger) + 1\right]|0\rangle, \tag{A3}$$

where $|0\rangle$ means the vacuum state $|0\rangle = |00\rangle_{c_1c_2}|00\rangle_{b_1b_2}$, and the term $c_2^\dagger b_2^\dagger c_1^\dagger b_1^\dagger|0\rangle$ has been neglected due to the low scattering probability. When there is a click in the photondetector D_6 or D_7, the projected state of the mechanical oscillator 1 and 2 is

$$|\psi\rangle_{b_1b_2}^\pm = \frac{1}{\sqrt{2}}\big(|1\rangle_{b_1}|0\rangle_{b_2} \pm |0\rangle_{b_1}|1\rangle_{b_2}\big). \tag{A4}$$

The above Bell states are usually used for quantum communications.

[1] A. K. Ekert, Phys. Rev. Lett. **67**, 661 (1991).
[2] C. H. Bennett, G. Brassard, and N. D. Mermin, Phys. Rev. Lett. **68**, 557 (1992).
[3] X. H. Li, F. G. Deng, and H. Y. Zhou, Phys. Rev. A **78**, 022321 (2008).
[4] C. H. Bennett, G. Brassard, C. Crepeau, R. Jozsa, A. Peres, and W. K. Wootters, Phys. Rev. Lett. **70**, 1895 (1993).
[5] G. L. Long and X. S. Liu, Phys. Rev. A **65**, 032302 (2002).
[6] F. G. Deng, G. L. Long, and X. S. Liu, Phys. Rev. A **68**, 042317 (2003).

[7] C. Wang, F. G. Deng, Y. S. Li, X. S. Liu, and G. L. Long, Phys. Rev. A **71**, 044305 (2005).
[8] W. Zhang, D. S. Ding, Y. B. Sheng, L. Zhou, B. S. Shi, and G. C. Guo, Phys. Rev. Lett. **118**, 220501 (2017).
[9] C. H. Bennett and S. J. Wiesner, Phys. Rev. Lett. **69**, 2881 (1992).
[10] X. S. Liu, G. L. Long, D. M. Tong, and F. Li, Phys. Rev. A **65**, 022304 (2002).
[11] C. H. Bennett, H. J. Bernstein, S. Popescu, and B. Schumacher, Phys. Rev. A **53**, 2046 (1996).
[12] T. Yamamoto, M. Koashi, and N. Imoto, Phys. Rev. A **64**, 012304 (2001).
[13] Z. Zhao, J. W. Pan, and M. S. Zhan, Phys. Rev. A **64**, 014301 (2001).
[14] Y. B. Sheng, F. G. Deng, and H. Y. Zhou, Phys. Rev. A **77**, 062325 (2008).
[15] X. H. Li and S. Ghose, Phys. Rev. A **91**, 062302 (2015).
[16] A. Botero and J. Mejía, Phys. Rev. A **98**, 032326 (2018).
[17] B. C. Ren, F. F. Du, and F. G. Deng, Phys. Rev. A **88**, 012302 (2013).
[18] Y.-B. Sheng, L. Zhou, and S.-M. Zhao, Phys. Rev. A **85**, 042302 (2012).
[19] Y. B. Sheng, L. Zhou, S. M. Zhao, and B. Y. Zheng, Phys. Rev. A **85**, 012307 (2012).
[20] F. G. Deng, Phys. Rev. A **85**, 022311 (2012).
[21] C. Wang, Phys. Rev. A **86**, 012323 (2012).
[22] H. Zhang and H. Wang, Phys. Rev. A **95**, 052314 (2017).
[23] H. Zhang, A. Alsaedi, T. Hayat, and F. G. Deng, Ann. Phys. **391**, 112 (2018).
[24] Y. B. Sheng and L. Zhou, Phys. Rev. A **98**, 052343 (2018).
[25] C. Y. Li and Y. Shen, Opt. Express **27**, 13172 (2019).
[26] H. Xu, L. Y. Jiang, A. A. Clerk, and J. G. E. Harris, Nature (London) **568**, 65 (2019).
[27] H. Xu, D. Mason, L. Jiang, and J. G. E. Harris, Nature (London) **537**, 80 (2016).
[28] H. Flayac and V. Savona, Phys. Rev. Lett. **113**, 143603 (2014).
[29] M. J. Woolley and A. A. Clerk, Phys. Rev. A **89**, 063805 (2014).
[30] J. Li, I. M. Haghighi, N. Malossi, S. Zippilli, and D. Vitali, New J. Phys. **17**, 103037 (2015).
[31] C. F. Ockeloen-Korppi, E. Damskägg, J.-M. Pirkkalainen, M. Asjad, A. A. Clerk, F. Massel, M. J. Woolley, and M. A. Sillanpää, Nature (London) **556**, 478 (2018).
[32] R. Riedinger, A. Wallucks, I. Marinković, C. Löschnauer, M. Aspelmeyer, S. Hong, and S. Gröblacher, Nature (London) **556**, 473 (2018).
[33] M. Aspelmeyer, T. J. Kippenberg, and F. Marquardt, Rev. Mod. Phys. **86**, 1391 (2014).
[34] M. Ludwig, A. H. Safavi-Naeini, O. Painter, and F. Marquardt, Phys. Rev. Lett. **109**, 063601 (2012).
[35] P. L. Yu, K. Cicak, N. S. Kampel, Y. Tsaturyan, T. P. Purdy, R. W. Simmonds, and C. A. Regal, Appl. Phys. Lett. **104**, 023510 (2014).
[36] Y. Tsaturyan, A. Barg, E. S. Polzik, and A. Schliesser, Nat. Nanotechnol. **12**, 776 (2017).
[37] R. N. Patel, Z. Wang, W. Jiang, C. J. Sarabalis, J. T. Hill, and A. H. Safavi-Naeini, Phys. Rev. Lett. **121**, 040501 (2018).
[38] S. M. Meenehan, J. D. Cohen, G. S. MacCabe, F. Marsili, M. D. Shaw, and O. Painter, Phys. Rev. X **5**, 041002 (2015).
[39] K. Stannigel, P. Komar, S. J. M. Habraken, S. D. Bennett, M. D. Lukin, P. Zoller, and P. Rabl, Phys. Rev. Lett. **109**, 013603 (2012).
[40] Y. D. Wang and A. A. Clerk, Phys. Rev. Lett. **108**, 153603 (2012).
[41] L. Tian, Phys. Rev. Lett. **108**, 153604 (2012).
[42] J. Chan, T. P. M. Alegre, A. H. Safavi-Naeini, J. T. Hill, A. Krause, S. Gröblacher, A. Markus, and O. Painter, Nature (London) **478**, 89 (2011).
[43] Y. C. Liu, Y. F. Xiao, X. Luan, and C. W. Wong, Phys. Rev. Lett. **110**, 153606 (2013).
[44] F. C. Lei, M. Gao, C. G. Du, Q. L. Jing, and G. L. Long, Opt. Express **23**, 11508 (2015).
[45] H. Zhang, X.-K. Song, Q. Ai, H. Wang, G.-J. Yang, and F.-G. Deng, Opt. Express **27**, 7384 (2019).
[46] E. R. MacQuarrie, T. A. Gosavi, N. R. Jungwirth, S. A. Bhave, and G. D. Fuchs, Phys. Rev. Lett. **111**, 227602 (2013).
[47] P. Ovartchaiyapong, K. W. Lee, B. A. Myers, and A. C. B. Jayich, Nat. Commun. **5**, 4429 (2014).
[48] D. A. Golter, T. Oo, M. Amezcua, K. A. Stewart, and H. L. Wang, Phys. Rev. Lett. **116**, 143602 (2016).
[49] D. A. Golter, T. Oo, M. Amezcua, I. Lekavicius, K. A. Stewart, and H. L. Wang, Phys. Rev. X **6**, 041060 (2016).
[50] E. R. MacQuarrie, M. Otten, S. K. Gray, and G. D. Fuchs, Nat. Commun. **8**, 14358 (2017).
[51] M. V. Gustafsson, T. Aref, A. F. Kockum, M. K. Ekström, G. Johansson, and P. Delsing, Science **346**, 207 (2014).
[52] M. J. A. Schuetz, E. M. Kessler, G. Giedke, L. M. K. Vandersypen, M. D. Lukin, and J. I. Cirac, Phys. Rev. X **5**, 031031 (2015).
[53] A. H. Safavi-Naeini and O. Painter, New J. Phys. **13**, 013017 (2011).
[54] H. Okamoto, A. Gourgout, C.-Y. Chang, K. Onomitsu, I. Mahboob, E. Y. Chang, and H. Yamaguchi, Nat. Phys. **9**, 480 (2013).
[55] M. C. Kuzyk and H. Wang, Phys. Rev. X **8**, 041027 (2018).
[56] M. A. Lemonde, S. Meesala, A. Sipahigil, M. J. A. Schuetz, M. D. Lukin, M. Loncar, and P. Rabl, Phys. Rev. Lett. **120**, 213603 (2018).
[57] T. S. Yin, X. Y. Lü, L. L. Wan, S. W. Bin, and Y. Wu, Opt. Lett. **43**, 2050 (2018).
[58] J. Q. Liao, J. F. Huang, L. Tian, L. M. Kuang, and C. P. Sun, arXiv:1802.09254.
[59] T.-Y. Chen, W.-Z. Zhang, R.-Z. Fang, C.-Z. Hang, and L. Zhou, Opt. Express **25**, 10779 (2017).
[60] B. Pepper, R. Ghobadi, E. Jeffrey, C. Simon, and D. Bouwmeester, Phys. Rev. Lett. **109**, 023601 (2012).